

Utilizing Satellite Data for Evaluation and Forecasting Applications at Astronomical Sites

D. André Erasmus & Marc Sarazin

*erasmus@sao.ac.za, South African Astronomical Observatory, P.O.
Box 9, Observatory 7935, South Africa.*

*msarazin@eso.org, European Southern Observatory,
Karlschwarzschildstr.2 D85748 Garching, Germany.*

Abstract. The observing quality on large telescopes at optical, infra-red and radio wavelengths is determined in large measure, by atmospheric transparency. An objective assessment of transparency at candidate sites should therefore be made before site selection. Additionally, once a telescope is operational, variations in atmospheric transparency continue to impact telescope performance on a daily basis. In operational mode, forecasts of observing quality can therefore be a valuable aid in telescope scheduling. In this paper weather satellite data suitable for monitoring and forecasting applications at astronomical sites is described and the methodology for cloud cover, water vapor and (clear sky) transparency measurement is explained. To demonstrate the successful application of these data, results from selected current and recent projects are presented.

1. Introduction

The performance of large telescopes at optical, infra-red and radio wavelengths is critically dependent on atmospheric transparency which is largely determined by cloud cover and water vapor. A quantitative survey of these conditions at potential telescope sites is therefore an essential precursor to site selection. Once an observatory has been developed at a particular site, cloud cover and water vapor continue to impact observations on a daily basis. In the latter case, cloud cover and water vapor forecasts can be a valuable aid in telescope scheduling.

Existing and potential astronomical sites tend to be located in remote areas where conventional meteorological observations are absent or scarce. The identification of potential telescope sites and the comparison of candidate sites for a particular telescope has in the past proven to be a difficult task. In order to make *in situ* measurements, a significant on-the-ground effort is required both in terms of manpower and equipment. Knowing what is involved has discouraged many an organization in their search for a telescope site.

Meteorological satellites, particularly those in geostationary orbit are a very useful source of data for astronomical site characterization. These satellites monitor cloud cover and water vapor over large sections of the globe with a spatial and radiometric resolution suitable for evaluation and forecasting applications at astronomical sites. Satellite data archives now comprise 10 or more years of

data coverage for many areas, providing an adequate climatological database for site evaluation and comparison. In addition, real-time satellite data can be used in combination with forecasted parameter fields from numerical meteorological models to produce forecasts of cloud cover and water vapor at observatory sites.

This paper provides an overview of weather satellite data coverage for different areas of the globe and describes the characteristics of these data relevant to monitoring and forecasting applications at astronomical sites. The methodology for cloud cover and water vapor measurement is described. To demonstrate the successful application of this methodology, results from current projects that aim to identify potential telescope sites in Northern Chile for Cerro Tololo Inter-American Observatory (CTIO) and to compare sites in the southwestern U.S.A. for Rocky Mountain Observatories Consortium (RMOC) are presented in brief. In addition, an assessment of the accuracy of cloud cover and water vapor forecasts being made operationally for European Southern Observatory telescope sites at La Silla and Paranal is presented. In line with the stated scientific goals of the IAU SITE 2000 workshop, the use of weather satellite data to identify potential astronomical sites around the globe is considered.

2. Satellite Data

Geostationary meteorological satellites provide excellent coverage of the globe particularly in low and middle latitudes. Figure 1 shows a nearly simultaneous view of the earth from four of these satellites located at 0° (Meteosat-7), 75° W (GOES-8), 135° W (GOES-10) and 140° E (GMS). These satellites provide a consistent measurement over large areas thus allowing for quantitative area surveys and objective site inter-comparisons. Measurements between satellites are also compatible.

The primary observing channels (passive remote sensing) are: infra-red window ($\sim 10.7 \mu\text{m}$), water vapor channel ($\sim 6.7 \mu\text{m}$) and visible ($\sim 0.55 \mu\text{m}$). Newer satellites also have near-infrared ($\sim 3.7 \mu\text{m}$), split (IR) window ($\sim 12.0 \mu\text{m}$) and a second water vapor channel ($\sim 7.3 \mu\text{m}$). These observations can be used separately and in combination to quantify cloud cover and water vapor in the atmosphere. The primary focus in this paper is on the use of $6.7 \mu\text{m}$ (water vapor) and $10.7 \mu\text{m}$ (IR window) imagery.

Temporally, these satellites monitor the full earth disk at least every three hours (some areas are covered more frequently). This enables resolution of the diurnal cycle of cloud cover and water vapor. In terms of the available archive, many areas of the globe now have coverage for 10 or more years so a suitable climatology can be constructed.

The spatial resolution (nadir footprint) varies according to channel, *viz.* $1 \text{ km} \times 1 \text{ km}$ in the visible, $4 \text{ km} \times 4 \text{ km}$ in the infrared window channel and $4 \text{ km} \times 8 \text{ km}$ (effectively $8 \times 8 \text{ km}$) in the water vapor channel. For many applications a reduced resolution will suffice (see section 3.). Such a data set has been and is being produced as part of the International Satellite Cloud Climatology Project (ISCCP). For ISCCP, the raw data are sampled so that the effective pixel resolution for all channels is $9.1 \text{ km} \times 8.0 \text{ km}$.

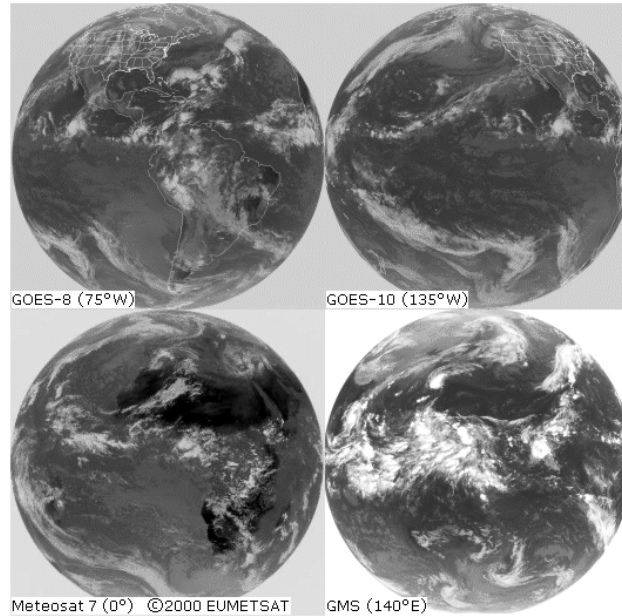


Figure 1. Primary geostationary meteorological satellites around the globe. Images are for the infra-red window channel ($\sim 11 \mu\text{m}$), all taken within 30 minutes of 11:30 UT on October 25, 2000.

3. Methodology

Measurements of water vapor and cloud are made by meteorological satellites by passive remote sensing at different wavelengths. Depending on the wavelength of the emissions being measured by the satellite, different quantities can be derived. Figure 2 shows the weighting functions for different infrared channels. In the IR window channel ($10.7 \mu\text{m}$), for example, emissions reach the satellite essentially unattenuated by the atmosphere so that radiance values measured are due to emission from the surface. However, if clouds are present in the atmosphere, these absorb and emit as blackbodies at infrared wavelengths. The result is that when clouds are present, they behave essentially as an elevated emitting “surface” so that radiation reaching the satellite is from the cloud top. Water vapor in the atmosphere is absorbent at most infrared wavelengths. The absorptivity for a given wavelength determines the layer in the atmosphere in which out-going terrestrial radiation will be absorbed and re-emitted by resident water vapor. Figure 2 indicates that observations at $6.7 \mu\text{m}$ are sensitive to emission by water vapor in the layer between 600 mb and 300 mb. (There are only small amounts of water vapor above 300 mb.) Emission from this layer depends on the amount of water vapor in the layer and temperature. Temperature can be accounted for by using an observed or representative temperature-height sounding so that emission is then only a function of the amount of the emitting gas, in this case water vapor, in the layer.

3.1. Conversion of Radiance to Brightness Temperature

Conversion of satellite infrared radiance measurements to meteorological quantities starts with computation of the observing channel brightness temperature.

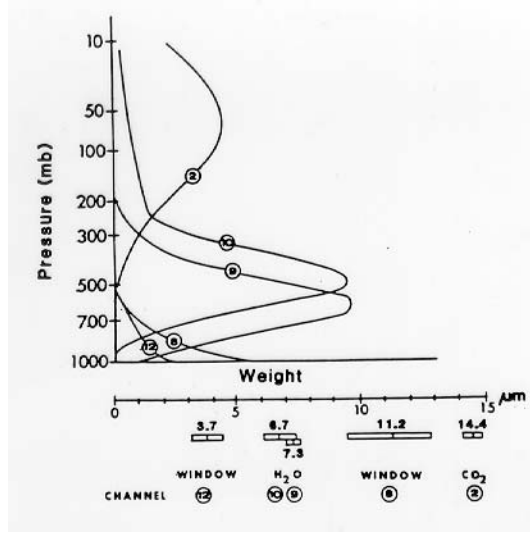


Figure 2. Weighting functions for selected infra-red observing channels (from Rao et al., 1990).

Radiance counts are 10-bits in length for the imager channels. In order to maintain compatibility with older data sets these have been scaled into 8-bit counts in the ISCCP data. The infrared channel calibration consists of a bias scaling factor and a first order gain scaling factor. True radiance values are obtained using the equation:

$$R = (X - b)/m \quad (1)$$

where R is radiance ($\text{mW}/[\text{m}^2 \text{sr cm}^{-1}]$) and X is the count value. The coefficients b and m are the scaling bias and the scaling gain, respectively.

The brightness (or effective) temperature is then obtained by inverting the Planck function as follows:

$$T_{eff} = (c_2 \cdot \nu) / \ln(1 + [c_1 \cdot \nu^3]/R) \quad (2)$$

where T_{eff} is effective temperature (K), “ln” stands for natural logarithm and ν (cm^{-1}) is the central wave number of the channel. The coefficients c_1 and c_2 are the two radiation constants and have values of $c_1 = 1.191066 \times 10^{-5}$ ($\text{mW m}^{-2} \text{sr}^{-1} \text{cm}^4$) and $c_2 = 1.438833$ (cm K). For the IR window channel, in order to get an accurate temperature of the emitting surface, R must be adjusted to account for absorption by water vapor between the surface and the satellite. In dry areas this adjustment is typically small. R^* , the adjusted radiance depends on the precipitable water vapor (PWV) and is given by $R^* = R/\text{Tr}$ where:

$$\text{Tr} = -0.0163(\text{PWV}) + 1.0119. \quad (3)$$

To convert effective temperature to actual temperature $T(\text{K})$, the following formula is used:

$$T = bT_{eff} + a. \quad (4)$$

The constants a (K) and b depend on the observation channel. These are bias and gain adjustments that account for variations in the inverse Planck function across the spectral passband of the channel. The differences between the values of T and T_{eff} increase with decreasing temperature. They are usually of the order of 0.1 K and hence negligible for most calculations.

Since the emissivity of land, water and clouds is near unity for infra-red wavelengths, the temperature thus computed from the satellite radiance values at $10.7 \mu\text{m}$ is a direct measurement of the temperature of the emitting surface. When clouds are present, the temperature is that of the cloud top which will be similar to the temperature of the air at the same altitude. If a temperature-height sounding is used then the height of the cloud can be determined. This technique has general applicability but breaks down near the surface since cloud at the surface will have a temperature similar to that of the surface. Also, under certain meteorological conditions, occurring notably on clear winter nights, the surface cools strongly and will be colder than the air above the ground. Under such conditions care must be taken not to interpret the cold ground as cloud at some height above the surface. To circumvent this problem, it is necessary to avoid “looking” below the altitude where the free air temperature is warmer than the ground temperature.

This is accomplished by first determining a “surface” temperature (T_s) for each location in the satellite image. Using digitized surface terrain heights and the nearest rawinsonde sounding, T_s can be estimated. Of course, if specific sites are being studied and a measured surface temperature is available then that measurement can be used for T_s . Once T_s is determined, a threshold temperature (T_t) for cloud detection must be derived. Even if the surface temperature is accurately known, T_t is set a few degrees colder than T_s to guarantee that the ground is not mistaken for low cloud under clear conditions. If a mean rawinsonde sounding is used to estimate T_s , these typically include the standard deviation of the temperature (σ_T) at each pressure (altitude) level so that σ_T at the “surface” can be interpolated. Air temperature data are normally distributed so more than 99% of the time temperatures will be within $3\sigma_T$ of the mean. Thus an estimate can be made of the “surface” cold temperature extreme (T_e) as follows: $T_e = T_s - 3\sigma_T$. $T_t = T_e$ may then be used as the threshold for cloud detection in the IR window analysis. If the satellite derived (brightness) temperature T_{ir} at $10.7 \mu\text{m}$ is colder than T_t then the existence of an emitting surface (cloud) above the site is indicated.

3.2. Conversion of $6.7 \mu\text{m}$ Brightness Temperature to UTH

The Upper Tropospheric Humidity (UTH) is a measure of the relative humidity of a layer extending approximately from 600 mb to 300 mb. For GOES data, Soden & Bretherton (1993, 1996) found a semi-empirical relationship between UTH and $6.7 \mu\text{m}$ channel brightness temperature in clear areas. The basic form of the relationship is:

$$\text{UTH} = [\exp(a + bT) \cdot \cos(q)]/p_0, \quad (5)$$

where q is the satellite viewing zenith angle, a and b are the least squares fit slope and intercept of the regression line as defined by the empirical relationship and p_0 is a normalized pressure variable.

$$p_0 = p(T = 240\text{K})/300, \quad (6)$$

where p (in mb) is the pressure level where the temperature (T) is 240 K. The values for a and b are seasonally dependent and are obtained from a table listing their values for each month of the year.

3.3. Computation of Precipitable Water Vapor

The computation of precipitable water vapor (PWV) follows from UTH. Since the UTH is a measure of the relative humidity in the layer between 300 mb and 600 mb, for pressure levels between 300 mb and 600 mb the relative humidity is set equal to the UTH. The corresponding mixing ratio (x), the mass of water vapor per mass of air (Kg/Kg), at each level can then be computed as follows:

$$x = \text{UTH} \cdot x_s \quad (7)$$

x_s , the saturation mixing ratio, is the maximum water vapour carrying capacity of the air at a given temperature and pressure. It can be computed via a complex algorithm, not described here, using the rawinsonde data.

The next step in the computation of PWV are the mixing ratio values for pressure levels below 300 mb and above 600 mb. Figure 3 shows the Denver mean monthly mixing ratio profiles for four months of the year in 1993. The profiles exhibit good linearity with pressure (height) below 600 mb. It is also clear that the contribution to total PWV from levels above 300 mb is small. To obtain the unknown mixing ratio values the computed values at 300 mb and 600 mb may respectively be scaled to lower and higher pressure levels. Since 700 mb corresponds to an altitude of approximately 3 000 m, for the purposes of PWV computations above most telescope sites, it will therefore not be necessary to perform large extrapolations. Once the mixing ratio profile is obtained, then,

$$\text{PWV} = (1/g) \int_0^p x \, dp, \quad (8)$$

where dp is the incremental pressure change with height in Pascals and g is the gravity acceleration constant. The units for PWV are then kg m^{-2} or mm of water.

In a study by Erasmus & Stanko (1997), it was found that the mean absolute difference between the measurements of PWV made at the Paranal Observatory in Northern Chile using a dark sky emissivity meter looking upwards, by the rawinsonde sounding at the city of Antofagasta (100 km to the north) and by the Meteosat-3 satellite using the pixel coincident with the observatory site, is less than 1 mm. This is within the range of respective instrument's error. Further, since different sampling (time and space) is used by each of the three methods, the level of agreement is remarkable. The methodology described above is superior to that used by Erasmus & Stanko (1997).

3.4. Cloud Detection and Classification

Cirrus (high altitude) clouds and their thickness may be inferred from the $6.7 \mu\text{m}$ imagery since they are found at an altitude (9–12 km) higher than the water vapor emission layer described above. The presence of cirrus clouds will produce

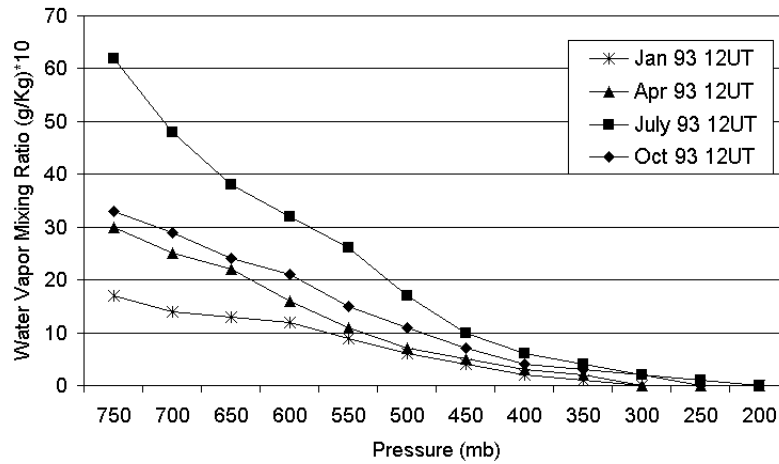


Figure 3. Mean monthly mixing ratio versus pressure (height) profiles as determined from the Denver rawinsonde for January, April, July and October 1993.

very low water vapor brightness temperature values and large ($>100\%$) UTH values. IR radiation from water vapor below the 300 mb level is absorbed and re-emitted at colder temperatures by the clouds, the amount of transmission through the cloud being dependent on cloud thickness. Pixels may be classified as clear, having opaque cirrus or having transparent cirrus based on the brightness temperature or UTH value for that pixel. The threshold brightness temperatures and UTH values are established empirically by comparison with independent ground-based measurements and are currently under review (see section 7.). Since the $6.7\ \mu\text{m}$ channel is only sensitive to cloud above the water vapor emission layer, cloud below about 450 mb cannot be detected in the $6.7\ \mu\text{m}$ imagery.

Since the atmosphere is essentially transparent in the IR window region (Figure 2) cloud can also be detected using the satellite IR channel centered at $10.7\ \mu\text{m}$ as described in section 3.1. An effective procedure for cloud detection uses observations made at both $6.7\ \mu\text{m}$ and $10.7\ \mu\text{m}$. First, the $6.7\ \mu\text{m}$ imagery is used to determine the existence of transparent or opaque cirrus at high altitude. If a pixel is determined to have opaque cirrus then the final cloud cover classification for that pixel location is “opaque” since the corresponding pixel in the $10.7\ \mu\text{m}$ would also give an opaque signature. However, if a pixel is either clear or transparent from the $6.7\ \mu\text{m}$ image analysis, the corresponding pixel in the $10.7\ \mu\text{m}$ image is examined. If cloud is detected in that pixel then the pixel location is classified as opaque. If not, then pixel locations classified respectively as clear or transparent remain clear or transparent. It should be noted that low cloud and ground fog cannot be detected unambiguously using the above methodology since they are of a similar temperature to the surface.

The sky cover classifications described in the previous paragraph are the extent of those possible for individual pixels. However, for a cluster of pixels further refinements can be made. For example, the nine pixel area shown in

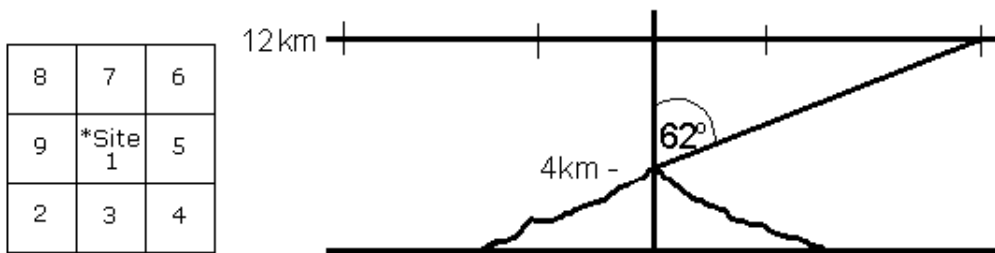


Figure 4. Schematic showing a 9-pixel area centered on a telescope site in plan view (left) and cross-section (right). At left, each square represents a $10 \text{ km} \times 10 \text{ km}$ pixel in the satellite image. At right, assuming a site altitude of 4 km, at Tropopause level (approximately 12 km), the “sky” encompassed by the 9-pixels corresponds approximately to an area of observation within 62° of zenith.

Figure 4 may be used to represent the astronomical observing “sky” above a particular location.

The number of pixels within the area for each single-pixel cloud cover category (see above) can be counted and that count used to provide a more accurate measure of observing conditions. If all nine pixels in the site area are simultaneously clear one can be fairly confident that observing conditions are indeed photometric (except for the possibility of the only cloud being ground fog or low cloud). For the results presented in section 5., the following classification scheme of cloud cover and observing conditions was used:

Clear (Photometric): All 9 pixels are clear

Transitional (Spectroscopic): 6–8 pixels are clear (1–3 pixels are transparent or opaque)

Opaque (Unsuitable for astronomy): 5 or fewer pixels are clear

4. Area Analysis

Using the methodology described above it is possible to map cloud cover and water vapor conditions over an area of interest. One of the aims of a study being conducted for CTIO, currently in progress, is to map cloud cover and water vapor over northern Chile using five years of satellite data from ISCCP. Satellite images of the study area are shown at actual spatial resolution in Figure 5.

Batch processing of the images permits computation of cloud cover and PWV statistics. For example, Figure 6 shows the aerial distribution of the percentage of clear skies and the median PWV for the period January 1995 to February 1996.

5. Comparative Site Analysis

In addition to area mapping, satellite data can be used to compare cloud cover and water vapor conditions at specific sites quantitatively. A study for Rocky Mountain Observatories Consortium (RMOC) compared cloud cover and wa-

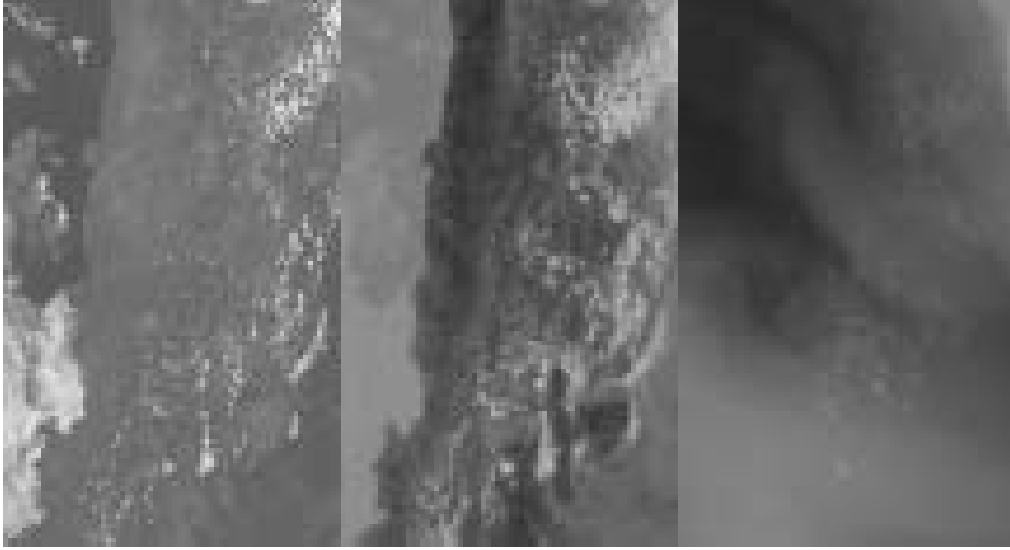


Figure 5. Visible (left), infrared window (center) and water vapor (right) channel images of the area 20.5° S to 30.5° S and 66° W to 72° W in Northern Chile on January 28, 1996 at 15:11 UT.

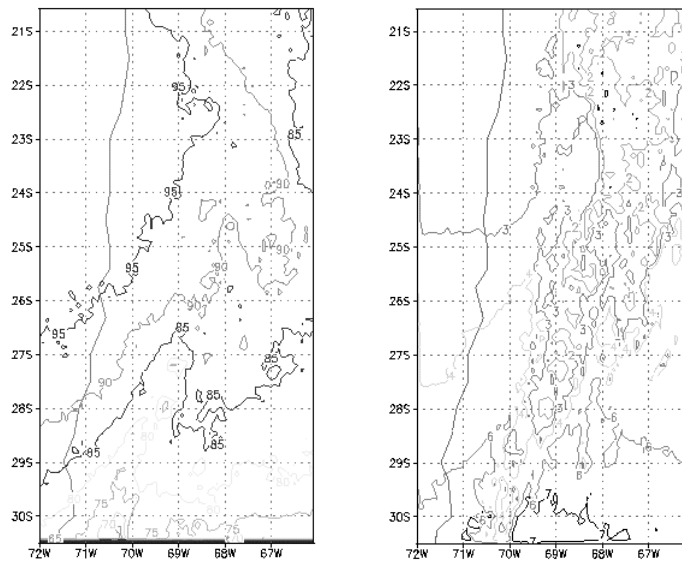


Figure 6. Percentage of clear skies (cloud at or above 400 mb, ~ 7500 m) for the first half of the observing night (left) and median PWV (mm) for water vapor above the surface or 700 mb, ~ 3000 m, for low terrain (right). Satellite data used are ISCCP from GOES-8 for the period January 1995 to February 1996.

ter vapor conditions at six sites in the southwestern U.S.A. (Erasmus, 2000) (Table 1). The data used in the comparison are $6.7\,\mu\text{m}$ and $10.7\,\mu\text{m}$ satellite imagery (every three hours) from ISCCP for the period July 1993 – February 1996. The rawinsonde data used as input are the mean monthly soundings (by year) for the stations of Denver, Tucson and Grand Junction.

Representative statistics of cloud cover and water vapor parameters were computed for the sites being surveyed. For the cloud cover analysis, the frequency of occurrence of cloud cover categories—clear, opaque and transitional—were derived. Water vapor conditions are indicated by PWV statistics such as the median, quartiles and 10th percentile values. The requirement for PWV computation is that all 9 pixels must be classified as clear. The “observing night” was defined to be the 12 hours from 22:00 LST (05:00 UT) to 10:00 LST (17:00 UT). Extension of the observing night into early morning daylight hours was done because RMOC was interested in quantifying conditions for infrared astronomy. In the study, seasonal and diurnal variations were characterized in some detail. However, only a sample of the main results is presented below to illustrate the type of information that can be obtained from the satellite measurements.

Table 1. Location data for the existing and potential telescope sites surveyed.

Pikes Peak	4 298 m	$38^{\circ}50'26''$ N	$105^{\circ}02'38''$ W
Mt. Evans	4 345 m	$39^{\circ}35'19''$ N	$105^{\circ}38'34''$ W
Mt. Graham	3 265 m	$32^{\circ}42'06''$ N	$109^{\circ}52'15''$ W
Mt. Lemmon	2 798 m	$32^{\circ}26'35''$ N	$110^{\circ}47'16''$ W
Jelm Mountain	2 943 m	$41^{\circ}05'50''$ N	$105^{\circ}58'35''$ W
Grand Mesa	3 180 m	$39^{\circ}04'00''$ N	$107^{\circ}56'10''$ W

The fraction of the time that conditions are clear (photometric), transitional (spectroscopic) and useable (sum of clear and transitional) during the observing night (22:00–10:00 LST) are shown in Figure 7 for the six sites. Other estimates of the percentage of useable nights at the Meyer-Womble Observatory on Mt. Evans (www.du.edu/~rstencil/MtEvans/SiteSurv.html#sec2) shows good agreement with the satellite measurement.

Table 2 shows the local variations in cloud cover for each site and indicates that local variability may be significant due to, for example, the influence of the surrounding topography. A steep gradient in cloudiness from south-west to north-east is observed at Grand Mesa and, to a much lesser extent, at Mt. Evans. This highlights the need for effective discrimination of cloud cover conditions over distances ~ 10 km when performing site evaluations.

Since the water vapor parameters are derived from satellite observations, they can only be computed under clear conditions. This makes sense from an astronomical point of view since, in general, clear skies are needed to make observations. PWV percentile values for the sites are shown in Figure 8. It is also clearly possible to obtain the complete PWV frequency distributions for the sites.

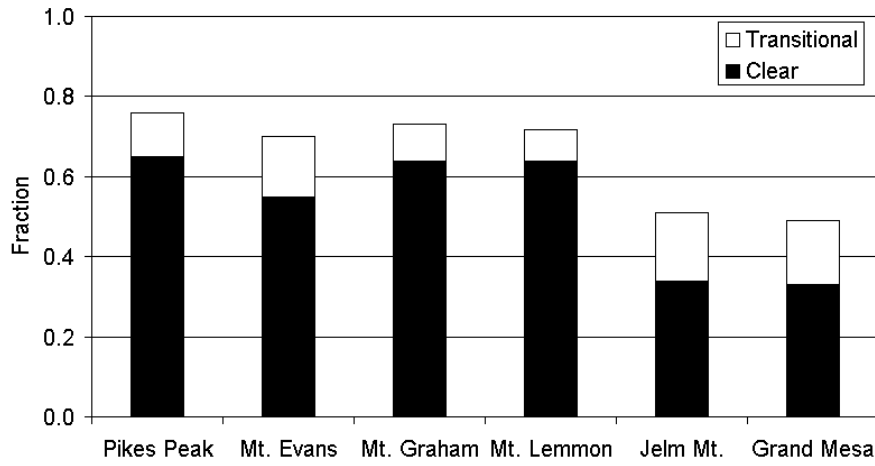


Figure 7. Fraction of time that sky cover conditions are clear (photo-metric) and transitional (spectroscopic) for the observing night (22:00–10:00 LST).

Table 2. Percentage opaque cloud (fraction of time unsuitable for astronomy) by pixel in the site areas (top is North, see Figure 4). Percentages apply to observing night (22:00–10:00 LST).

Pikes Peak			Mt. Evans			Mt. Graham		
22	21	21	26	25	24	25	25	25
22	22	21	29	26	25	25	25	25
21	21	21	28	28	27	24	24	24
Mt. Lemon			Mt. Jelmn			Grand Mesa		
26	26	25	46	44	47	47	53	57
26	26	25	48	44	48	43	45	51
25	26	25	50	44	46	39	43	50

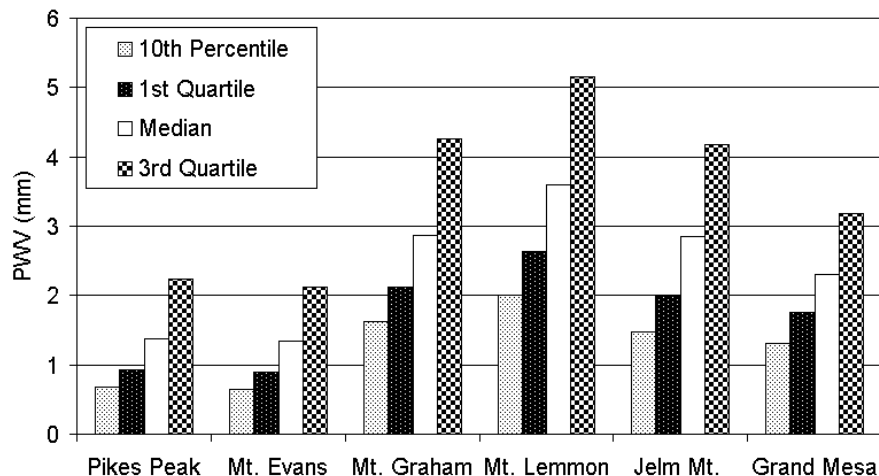


Figure 8. PWV percentile values at each site for the observing night (22:00–10:00 LST).

6. Cloud Cover and Water Vapor Forecasts

Satellite data, in combination with output from numerical meteorological forecast models, can be used to produce forecasts of cloud cover and water vapor at telescope sites. For example, cloud cover and water vapor forecasts for Paranal and La Silla Observatories are being made operationally using data from the GOES-8 satellite and meteorological forecast model data from the European Center for Medium-range Weather Forecasting (ECMWF) (Erasmus & Maartens, 1999; Erasmus & Sarazin, 2000). The data are obtained in real-time and ingested into a specially developed forecast program that produces an analysis and forecasts of cloud cover and water vapor conditions at the observatory sites (www.eso.org/gen-fac/pubs/astclim/forecast/meteo/ERASMUS/).

The two sources of input data are necessary to produce an accurate forecast. The ECMWF analysis of cloud cover was found to be unsuitable for cloud cover detection above Paranal with only 15–25% of cloudy nights identified. ECMWF humidity fields are also inadequate for determining PWV values with sufficient accuracy. For most meteorological applications, it is sufficient to resolve PWV values to within 1 cm. Consequently, the ECMWF model uses a smoothing technique when defining moisture fields. This makes it ineffective in discriminating moisture levels in very dry areas. Telescopes are generally located in these areas and PWV measurement to within 1 mm or better is needed for astronomical applications. Therefore, in the forecast program referred to earlier, the satellite is used to characterize the cloud cover and humidity fields and the forecasted fields of wind and geopotential height (pressure) from the ECMWF model are used to predict the movement of the cloud and water vapor. This approach is proving to be effective.

Output from the current operational version of the forecast program, which utilizes only $6.7\ \mu\text{m}$ satellite imagery, was compared to ground observer logs

of cloud cover and PWV measurements from a dark-sky emission monitor at Paranal. The comparison is based on forecasts (typically five per day at 3-hour intervals between 00 UT and 12 UT) made over the period August 26 – December 31, 1998. Each output consists of forecasts of cloud cover and PWV for eight 3-hour periods out to 24 hours.

For the water vapor forecasts the rms difference between the forecasted and observed (ground-based monitor) PWV values were computed. The rms difference is 0.4 mm for the first 3-hour forecast period, increases to 1.0 mm for the 9–12 hours forecast and reaches 1.3 mm for the 21–24 hours forecast period. As noted in section 3.3., rms differences between *observations* of PWV using various measurement methods are typically about 1.0 mm, so one can reasonably conclude that differences due to the measurement methods used are the dominant component of the forecast errors.

Using four cloud cover categories (Very Cloudy: >70% cloud cover, Cloudy: 33–70% cloud cover, Slightly Cloudy: 10–33% cloud cover and Clear: <10% cloud cover), the forecast was found to be accurate within one cloud cover category 89% of the time (1 395 pairs of observations) under all conditions (clear and cloudy). When only days with cloud present (according to the ground observer) are considered (79 pairs of observations), cloud forecasts agreed with observed cloudiness to within one cloud cover category 64% of the time. These results represented a significant improvement over what was possible using only the ECMWF forecasted fields.

In order to find out why the forecasts are sometimes missed under cloudy conditions and to see if improvements in the forecast methodology were possible, the *observed* satellite cloud cover was compared to the cloudiness as determined by the ground observer. It was found that the number of occasions that *observations* were in disagreement (cloud fraction differed by more than one category) was identical to the number of occasions forecasts were missed. Remarkably when there was disagreement, the disagreement was total (when the ground observer sees cloud the satellite sees none and vice versa). This suggested that the ground observer and satellite were seeing cloud differently. For 12/29 occurrences the satellite indicated the presence of transparent cirrus while the ground observer saw clear skies and 17/29 times the ground observer saw opaque cloud while the satellite indicated clear skies. The former discrepancy is clearly due to the thresholds used for transparent cirrus detection by the satellite. These are set too low so that the satellite is being oversensitive. Calibration of the satellite detection thresholds using an independent (astronomical) extinction measurement is needed. A study to do this is underway (see section 7.). The latter group of cases represents occasions when the cloud present is below the altitude (about 450 mb) at which it is detectable using $6.7\ \mu\text{m}$ imagery. By including the $10.7\ \mu\text{m}$ satellite data in the forecast, so that low and middle level cloud can be better detected, this problem is largely circumvented. An upgrade of the forecast program to include the use of $10.7\ \mu\text{m}$ imagery is expected to be completed early in 2001 and a re-verification of the forecast accuracy will follow.

7. Comparison of Satellite-Derived Transparency with Ground-Based Atmospheric Extinction Measurements

As noted in sections 3. and 6., the relationship between atmospheric transparency as determined from the satellite at $6.7\mu\text{m}$ and atmospheric transparency as observed from the ground at optical wavelengths is uncertain. It is reasonable to conclude that transparency should decrease as UTH increases since, as the UTH increases beyond a certain threshold, hydrometeors (haze particles, droplets and ice crystals) grow by condensation and deposition. On this premise a transparency index (TI) is defined when most of the sky is clear (less than 10% of the pixels are opaque) as the average of the clear and transparent pixel TI values where $\text{TI} = 1.0$ for clear pixels and $\text{TI} = 1 - (\text{UTH}_{\text{pixel}} - \text{UTH}_{\text{CT}}) / (\text{UTH}_{\text{TO}} - \text{UTH}_{\text{CT}})$ for transparent pixels. The quantities UTH_{CT} and UTH_{TO} are the threshold UTH values for discriminating clear from transparent and transparent from opaque, respectively.

However, without some direct measurement of atmospheric extinction, a calibration of satellite-derived transparency indicators is not possible. Over the last year a system to measure the photometric sky quality in real-time whenever the sky is clear enough for bright stars to be visible has been implemented at ESO Observatories at Paranal and La Silla. It is known as the *Line Of Sight Sky Absorption Monitor* (LOSSAM). The LOSSAM instrument is a 20 cm diameter telescope monitoring the flux from a bright star within 45 degrees of zenith and delivering estimates of the variability of the atmospheric extinction over 10 minute time intervals. Depending on the direction and speed of atmospheric motion, there may be more or less correspondence with the area of the sky above the site as sampled by the satellite. With no motion (not likely, since motion is usually from the west) the area sampled by LOSSAM in 10 minutes is very small. With movement to the east at 50 km/h the atmosphere would move approximately 8 km (one pixel width in $6.7\mu\text{m}$ image, two pixel widths in $10.7\mu\text{m}$ image). LOSSAM rms extinction is compared to the satellite-derived TI for the observatory sky which covers about 45 image pixels in a circular area centered over the site. Because of this difference in the sampling areas of each method, comparable results are expected only in cases when the cloud pattern is uniformly distributed in the sky.

From observing experience in astronomy, an rms atmospheric extinction lower than 0.01 magnitude corresponds to a perfectly photometric sky. In such conditions, the ratio of the absolute flux F_0 of a star to the actual flux F measured when observing through the atmosphere does not depend on the direction of observation but only on the zenith angle Y . The zenith dependency is characterized by an atmospheric extinction coefficient E for a given observing wavelength:

$$E = -2.5 \cos \Psi \cdot [\text{Log}(F) - \text{Log}(F_0)]. \quad (9)$$

A relationship between TI and E is defined for situations where the sky is not photometric but some type of astronomical observing, like spectroscopy, is still possible and where satellite-based forecasts of transparency would be of direct operational consequence. For these cases, ground-based measurements of

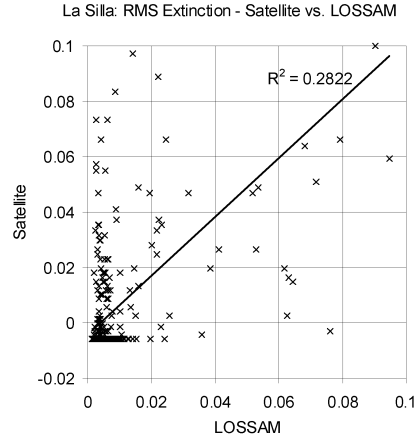


Figure 9. Satellite-derived atmospheric extinction (*Satrms*) versus LOSSAM extinction (*E*).

rms extinction ranged from 0.01 to 0.1 magnitude. The corresponding extreme TI values were 1.0 and 0.3.

Using data for the La Silla observatory over the period January–October 2000, 486 pairs of observations were obtained with 406 (83.5%) perfectly photometric ($E < 0.01$) and 80 (16.5%) with E in the range 0.01–0.1. A parameter *Satrms* is defined by the regression relationship between E and $\text{Log}(\text{TI})$ for non-photometric conditions as follows:

$$\text{Satrms} = -0.3137[\log(\text{TI}) + 0.0182] \quad (10)$$

Applying this relationship to the full data set, *Satrms* is plotted versus E in Figure 9. Table 3 summarizes the comparison.

The satellite-derived extinction parameter correctly discriminates between photometric and non-photometric conditions 86% (320/370) of the time. Closer examination of the 45 cases in which the satellite incorrectly indicates that conditions are non-photometric, shows that for most of these cases, *Satrms* was in the range 0.01–0.03. In other words, very close to the photometric threshold of $E = 0.01$. A slight adjustment in the definition of TI would therefore further improve the discrimination accuracy. This work is still in progress. Further refinements are possible using TI and other indices of transparency will also be considered.

Table 3. Satellite-derived atmospheric extinction (*Satrms*) and LOSSAM extinction (E) for photometric ($E < 0.01$) and non-photometric ($E > 0.01$) conditions. Refer to text for details.

LOSSAM	Satellite	
	<0.01	>0.01
<0.01	287	45
>0.01	5	33

8. Conclusion

It has been shown that satellite data can be used to evaluate and compare cloud cover and water vapor conditions at existing and potential telescope sites. These data also allow for area-mapping of cloud cover and water vapor in a manner that enables potential telescope sites to be found. Additionally, these data can be used in combination with numerical meteorological forecast model output to produce operational forecasts of atmospheric transparency with an accuracy suitable for use in the telescope scheduling process. Existing astronomical observatory sites, known to have excellent observing conditions, are becoming crowded. The number of undeveloped potential sites of similar quality are limited. In view of these facts, there is an urgent need to identify and characterize potential telescope sites globally for the future. Using satellite data and the methodology described and demonstrated in this paper this need can now be addressed.

Acknowledgments. This paper was compiled from research supported by European Southern Observatory, Cerro Tololo Inter-American Observatory and Rocky Mountain Observatories Consortium. D. S. Maartens, C. A. van Staden, P. R. Stanko and R. Peterson have participated in this research effort.

References

- Erasmus, D. A., & Maartens, D. S. 1999 in Operational Forecasts of Cirrus Cloud Cover and Water Vapor Above Paranal and La Silla Observatories. Final report, European Southern Observatories contract No. 2538/VPS/97/-9480/HWE
- Erasmus, D. A. 2000 in A Satellite Survey of Water Vapor and Cloud Cover at Selected Existing and Potential Telescope Sites in the Southwestern U.S.A. Rocky Mountain Observatories Consortium. Final Report December 31, 2000. 37pp
- Erasmus, D. A., & Sarazin, M. 2000 in Forecasting Precipitable Water Vapor and Cirrus Cloud Cover For Astronomical Observatories: Satellite image processing guided by synoptic model dissemination data. SPIE Conference on Image and Signal Processing for Remote Sensing IV. Paper SPIE-4168, Barcelona. 25–29 September, 2000
- Rao, P. K., Holmes, S. J., Anderson, R. K., Winston, J. S., & Lehr, P. E., Eds., 1990 in Weather Satellites: Systems, Data and Environmental Applications. American Meteorological Society, Boston, 503pp
- Soden, B. J., & Bretherton, F. P. 1993 in Upper tropospheric relative humidity from the GOES 6.7 μm channel: Method and climatology for July 1987. J. Geophys. Res. 96, 16 669–16 688
- Soden, B.J., & Bretherton, F. P. 1996 in Interpretation of TOVS water vapor radiances in terms of layer-average relative humidities: Method and climatology for the upper, middle and lower troposphere. J. Geophys. Res. 101, 9 333–9 343